Anastasia Kraskov, Johannes von Sass, Anh Duc Nguyen, Tu Oanh Hoang, David Buhrke, Sagie Katz, Norbert Michael, Jacek Kozuch, Ingo Zebger, Friedrich Siebert, Patrick Scheerer, Maria Andrea Mroginski, Nediljko Budisa, Peter Hildebrandt

Local electric field changes during the photoconversion of the bathy phytochrome Agp2

Local electric field changes during the photoconversion of the bathy phytochrome Agp2

Anastasia Kraskov[§1], Johannes von Sass[§1], Duc A. Nguyen[1], Tu Oanh Hoang[1], David Buhrke[1,6], Sagie Katz[1], Norbert Michael[1], Jacek Kozuch[3], Ingo Zebger[1], Friedrich Siebert[2], Patrick Scheerer[4], Maria Andrea Mroginski[1*], Nediljko Budisa[5*], Peter Hildebrandt[1]*

[1] Technische Universität Berlin, Institut für Chemie, Sekr. PC14, Straße des 17. Juni 135, D-10623 Berlin, Germany

[2] Albert-Ludwigs-Universität Freiburg, Institut für Molekulare Medizin und Zellforschung, Sektion Biophysik, Hermann-Herderstr. 9, D-79104 Freiburg, Germany

[3] Freie Universität Berlin, Fachbereich für Physik, Arnimallee 14, D-14195 Berlin, Germany

[4] Charité – Universitätsmedizin Berlin, corporate member of Freie Universität Berlin and Humboldt-Universität zu Berlin, Institute of Medical Physics and Biophysics, Group Protein X-ray Crystallography and Signal Transduction, Charitéplatz 1, D-10117 Berlin, Germany

[5] University of Manitoba, Department of Chemistry, 144 Dysart Rd, 360 Parker Building, R3T 2N2 Winnipeg, MB, Canada

[6] present address: University of Zürich, Department of Chemistry, Winterthurerstr. 190, CH-8057 Zürich, Switzerland

§ equal contributions to the work

* corresponding authors

Peter Hildebrandt: email: hildebrandt@chem.tu-berlin.de

Nediljko Budisa: email: Nediljko.Budisa@umanitoba.ca

Maria Andrea Mroginski: email: andrea.mroginski@tu-berlin.de

Abstract

Phytochromes switch between a physiologically inactive and active state via a light-induced reaction cascade, which is initiated by isomerization of the tetrapyrrole chromophore and leads to the functionally relevant secondary structure transition of a protein segment (tongue). Although details of the underlying cause-effect relationships are not known, electrostatic fields are likely to play a crucial role in coupling chromophore and protein structural changes. Here, we studied local electric field changes during the photoconversion of the dark state Pfr to the photoactivated state Pr of bathy phytochrome Agp2. Substituting Tyr165 and Phe192 in the chromophore pocket by *para*-cyanophenylalanine (pCNF), we monitored the respective nitrile stretching modes in the various states of the photoconversion (vibrational Stark effect). Resonance Raman and IR spectroscopic analyses revealed that both pCNF-substituted variants undergo the same photoinduced structural changes as wild-type Agp2. Based on a structural model for the Pfr state of F192pCNF, a molecular mechanical – quantum mechanical approach was employed to calculate the electric field at the nitrile group and the respective stretching frequency in excellent agreement with the experiment. These calculations serve as a reference for determining the electric field changes in the photoinduced states of F192pCNF. Unlike F192pCNF, the nitrile group in Y165pCNF is strongly hydrogen bonded such that the theoretical approach is not applicable. However, in both variants the largest changes of the nitrile stretching modes occur in the last step of the photoconversion, supporting the view that the proton-coupled restructuring of the tongue is accompanied by a change of the electric field.

Introduction

Phytochromes are sensory photoreceptors that use the ratio of light intensities as a source of information to initiate physiological processes.[1,2] The light-absorbing unit is a linear methine-bridged tetrapyrrole which is covalently bound to the protein in the photosensory core module (PCM) constituted by a PAS-GAF-PHY domain triade.[2] The PCM interconverts between the red absorbing Pr and far-red absorbing Pfr state, in which the chromophore adopts a *ZZZssa* and *ZZEssa* configuration, respectively. Phytochromes are found in plants, fungi, and bacteria. In eukaryotic and most bacterial phytochromes, Pr is the stable dark state (prototypical phytochromes), in contrast to bathy bacterial phytochromes, where Pfr is the thermally stable state. Despite different domain compositions and different types of tetrapyrrole chromophores, all phytochromes share common features of photoinduced reaction cascades (Figure 1).

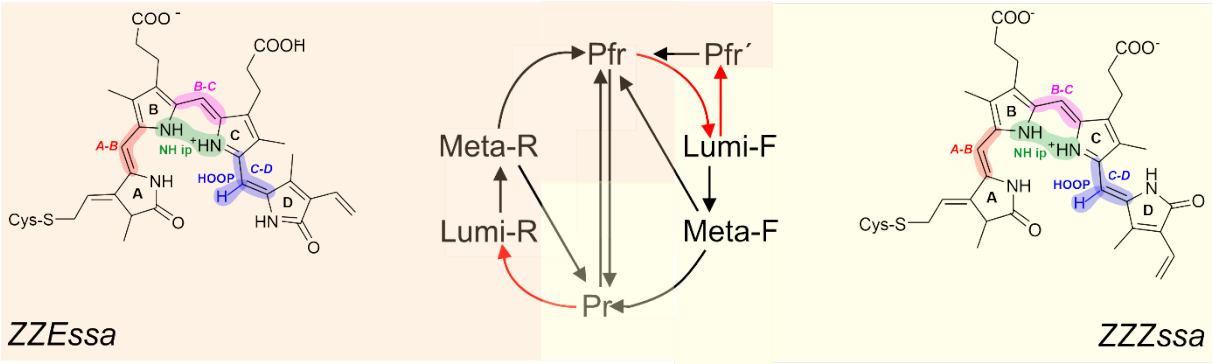

Figure 1. Simplified scheme of the photoinduced reactions in phytochromes. Photochemical and thermal reactions are indicated by red and black arrows, respectively. Further details are given in the Supporting Information (Fig. S3). The various states of phytochrome with the chromophore in the *ZZZssa* (right) and *ZZEssa* configuration (left) are highlighted by the yellow and red background color, respectively. The structural formulas also indicate the localization of important vibrational modes of the chromophore.

The photoinduced conversion between Pr and Pfr starts with double bond photoisomerization at the methine bridge between rings *C* and *D* to yield a distorted, energy-rich *ZZEssa* (Pr → Lumi-R) or *ZZZssa* (Pfr → Lumi-F) configuration, presumably with only minor structural adjustments of the amino acid residues near the chromophore isomerization site.[3] The primary processes are followed by chromophore relaxations and structural rearrangements in the chromophore binding pocket in the Meta-R and Meta-F states. The decay of the Meta states to the final photoconversion products is coupled with crucial protein structural changes. This primarily involves the secondary structure transition of the tongue, a peptide segment in the PHY domain.[4] In prokaryotic phytochromes, this transition represents an important step to communicate PCM activation or deactivation to the output module, often a histidine kinase.

Particularly detailed insights into the coupling between chromophore and protein structural changes in the PCM were gained for the bathy phytochrome Agp2 from *Agrobacterium fabrum*, based on crystal structures determined for the parent Pfr and the Meta-F states of the wild-type Agp2-PCM and its variant Agp2-PAiRFP2, and a large body of spectroscopic data (Figure 1).[5,6,7,8] The results indicate that *E* → *Z* photoisomerization of the biliverdin (BV; Figure 1) chromophore leads to reorientations of key amino acid residues in the chromophore binding pocket, accompanied by a reorganization of the extended hydrogen bond (H-bond) network around the chromophore. Eventually, a rotation of Tyr165 and Phe192 as well as a removal of a water molecule on ring *D* of BV leads to the movement of Gln190 towards Trp440 resulting in a destabilization of the coil region of the tongue.[5] However, a complete conversion of the tongue from the α-helical to the β-sheet structure requires the proton transfer from the propionic side chain of BV´s ring *C* (prop*C*) to His278, which occurs during the decay of Meta-F to Pr.[8] On the basis of spectroscopic studies of site-specifically engineered Agp2 variants and Agp2 adducts with BV monomethylester,[7,8] we suggested that proton translocation alters the overall

electrostatics in the chromophore binding pocket, which eventually drives the secondary structure transition of the tongue.

To test this hypothesis, we have exploited the vibrational Stark effect (VSE) which allows monitoring local electric field changes via frequency shifts of appropriate reporter groups.[9] Nitriles are of particular interest since their stretching modes can be observed in a spectral region free of any vibrational bands of the protein. This VSE reporter group can be introduced into protein structures via chemical modifications of thiol side chains,[10] or, as in this work, by the *in vivo* incorporation of a non-canonical amino acid (ncAA) via orthogonal translation.[11,12,13] Here we have employed the ncAA *para*-cyanophenylalanine (pCNF) to replace two amino acids at critical positions in the chromophore binding pocket, i.e. Tyr165 and Phe192. It is shown that both pCNF-containing variants undergo the complete Pfr $\rightarrow$ Pr photoconversion as the wild-type (WT) Agp2 such that it was possible to monitor electric field changes at different stages of the reaction cascade. The results reveal drastic changes of the electric field in the chromophore binding pocket concomitant with the deprotonation of prop*C* in the final Meta-F $\rightarrow$ Pr reaction step.

Methods

Protein expression and purification. The plasmid pEVOL_pCNF-RS harboring the orthogonal aminoacyl-tRNA synthetase/tRNA pair for *para*-cyanophenylalanine (pCNF)-incorporation[11] was co-transformed with pAG2-M2-F192amber or pAG2-M2-Y165amber into the engineered *E. coli* strains C321.ΔA.exp (DE3) or BL21 (DE3), respectively. Cell cultivation and protein purification were described in the Supporting Information (Sect. 1.1., Figure S1, S2).[5]

Spectroscopy. Resonance Raman (RR) measurements were performed using a Bruker Fourier-transform Raman spectrometer RFS 100/S with 1064 nm excitation (Nd-YAG cw laser,

line width 1 cm^{-1}), equipped with a nitrogen-cooled cryostat from Resultec (Linkam).[8] All spectra of the samples in frozen solution were recorded at ca. 90 K with a laser power at the sample of 690 mW and an accumulation time of typical one hour. In order to identify potential laser-induced damage of the phytochrome samples, RR spectra before and after a series of measurements were compared. In no case, changes between these control spectra were determined. Protein and buffer Raman bands were subtracted on the basis of a Raman spectrum of apo-phytochrome. To probe photoconversion products the sample was illuminated by a laser diode (λ = 785 or 660 nm) at 20° C. Residual contributions from the un-photolyzed state were removed by spectra subtraction using the OPUS software (Bruker). After photoconversion, the sample was cooled to 90 K for the Raman measurements.

IR spectroscopic measurements were carried out in the transmission mode at 25 °C using a Bruker Tensor 27 or IFS66v/s FTIR spectrometer.[8] IR spectra were recorded accumulating 200 single scans with a spectral resolution of 2 cm^{-1} in the range between 1000 and 3500 cm^{-1}. For IR difference spectroscopy, an optical filter with a cut-off frequency > 1850 cm^{-1} and the double-sided acquisition mode for the corresponding interferogram was used. The Pfr $\rightarrow$ Pr interconversion was achieved by the continuous illumination of the sample with built-in diode arrays (780 and 670 nm wavelength). The difference spectra were obtained by subtraction of the initial state spectrum from the illuminated state spectrum. Low-temperature IR spectra were measured as described elsewhere,[14] using protein concentrations of ca. 1 and 10 mM for IR difference spectra in the amide band region and IR absolute spectra in the nitrile stretching region, respectively.

Calculations. The crystal structures of wild-type Agp2-PCM in the Pfr state (PDB entry 6G1Y)[5] and the Agp2-PCM variant PAiRFP2 in the Meta-F state (PDB entry 6G20)[5] were used as template for generating the initial structure models of the F192pCNF and Y165pCNF mutants. Missing residues in the crystal structures were reconstructed by three-dimensional

homology modelling using SWISS MODEL.[15] The amino acid in Agp2-PAiRFP2 were manually replaced to match the Agp2 sequence as reported previously.[8]

In the computational Agp2-PCM models for the Pfr and Meta-F the propionic side chain *C* (prop*C*) as well as all four pyrrole rings were protonated according to previous spectroscopic observations.[6] Furthermore, hydrogens were added to the crystallographic structure according to predictions based on Karlsberg2+.[16] The highly conserved amino acids His248 and His278 were modeled as charge-neutral, each with a proton at Nε position.

Under the assumption that the primary event of the photoconversion is restricted to the isomerization of ring *D* without significant relaxation of the protein environment, an initial geometry for Agp2-PCM in the Lumi-F state was constructed using the crystal structure of Agp2-PCM in Pfr state as template and rotating ring *D* of the biliverdin 180 degrees while initially keeping the protein scaffold fixed.

Molecular dynamics (MD) simulations of the model systems were performed using the NAMD-V2.10 software, as described in detail in the Supporting Information (Sect. 1.2.).[17] After twenty nanoseconds fifty snapshots were extracted randomly from the trajectories and used as starting geometries for subsequent hybrid QM/MM calculations. Accordingly, the biliverdin chromophore, the side chains of Cys13, the Asp196, the pyrrole water as well the pCNF moiety replacing either Phe192 or Tyr165 were treated quantum mechanically at the B3LYP/6-31G* level of theory. The protein matrix, solvent water, and ions were described molecular mechanically using CHARMM36 force field.[18] The QM/MM optimized geometries were further used as input for subsequent frequency calculation of exclusively the QM fragment as described previously.[19]

Results

We have generated the Agp2-PCM variants F192pCNF and Y165pCNF. Thus, the VSE reporter group was introduced at two positions in the vicinity of the isomerization site (Figure 2). Tyr165 forms a H-bond with prop*C* in the Pfr state and is essential for the proton transfer to His278. Phe192 is part of the conformational switch that induces destabilization of the coil region of the tongue in the Meta-F state.

Structures of the Pfr states of F192pCNF and Y165pCNF. Both substitutions are structurally conservative and even the H-bond acceptor function of the hydroxyl group of Tyr165 is expected to be mimicked by the nitrile group of pCNF. This expectation is supported by structural models generated for the Pfr states of the Y165pCNF and F192pCNF variants (Figure 2). The structure of the BV backbone in the F192pCNF model remains practically identical to that in the crystal structure as reflected by the low RMSD value of 0.32 ± 0.03 Å computed for all heavy atoms of the BV backbone. The side chain prop*C*, however, reorients towards Ser262 in response to slight changes of the H-bond network caused by the F192pCNF mutation and the flow of additional water molecules into the chromophore binding pocket. These conformational changes around prop*C* are accompanied by reorientation of His278 and the hydroxyl group of Ser262. All other residues in the cavity largely remain at their crystallographic positions as in the crystal structure. The BV cofactor accommodates itself in the chromophore binding cavity by slightly twisting around the methine bridges as shown by the pyrrole tilt angles and methine bridge torsional angles listed in Table S3. The protein environment surrounding the mutated Phe192 (Figure 2B) is basically not affected by the incorporation of the reporter group. The largest displacements are predicted for the Gly173 and Phe167 (*vide infra*). Note that the reporter group is not involved in any H-bonding interactions with the environment.

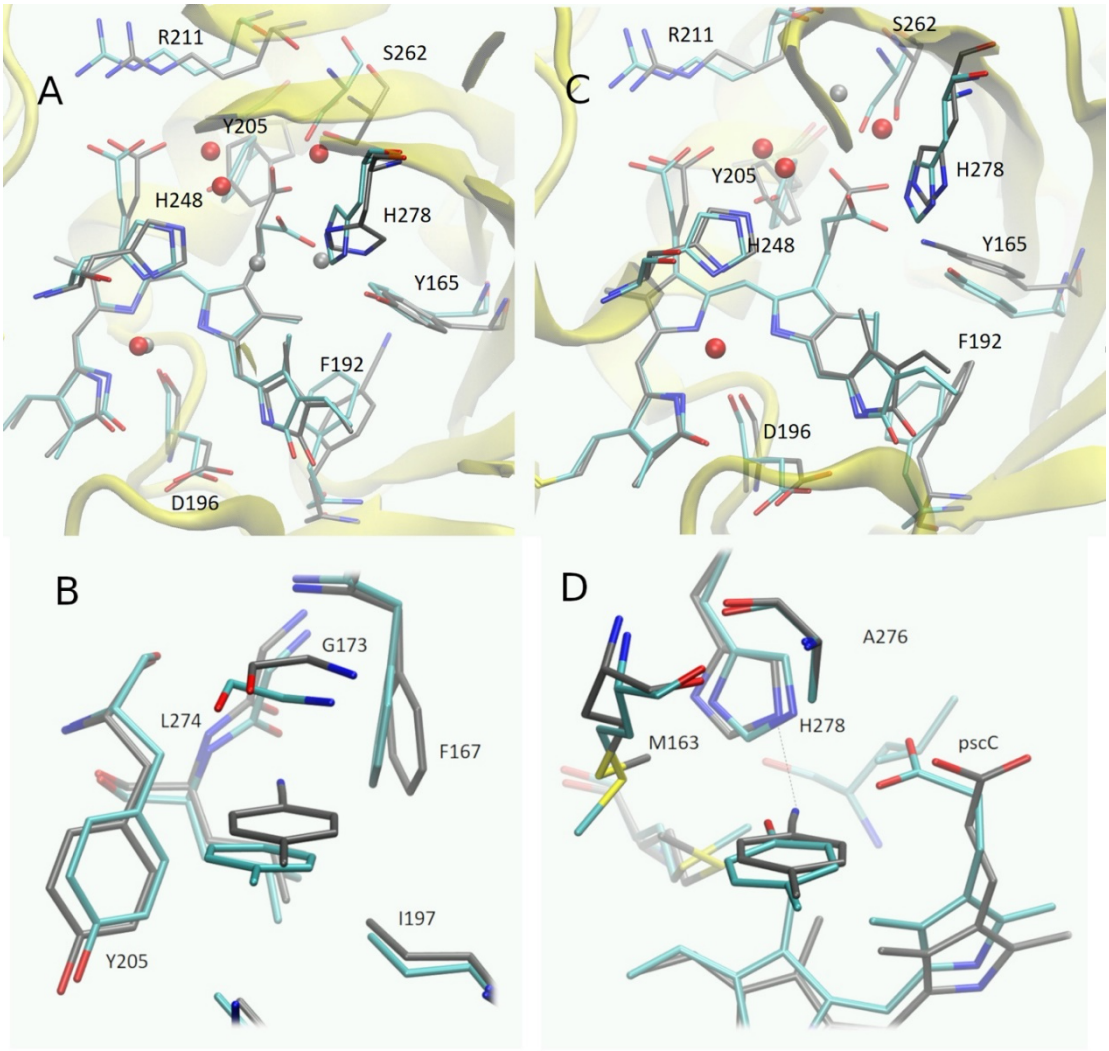

Figure 2. Representative structural models of the chromophore binding pocket of (**A**) F192pCNF and (**C**) Y165pCNF in the Pfr state, obtained by molecular modelling (gray), compared with the experimentally determined Pfr crystal structure of the WT Agp2-PCM (PDB entry 6G1Y)[5] (cyan). (**B**) and (**D**) show the environment around the reporter group in F192pCNF and Y165pCNF, respectively. The dotted line in (**D**) highlights the hydrogen bonding interaction between the nitrile and the His278 side chain. Red spheres represent water molecules present in the crystal structures while gray spheres represent water molecules present in the optimized structures. The representative structures correspond to optimized QM/MM snapshots of the MD trajectory for which the calculated stretching frequency of the nitrile is close to the average value computed for the corresponding ensemble of 50 snapshots. For the F192pCNF and Y165pCNF variants, we considered the structures with a nitrile stretching frequency of 2230.6 and 2238.7 cm^{-1}, respectively.

Similar to the F192pCNF model, substitution of the Tyr165 by pCNF has only a small effect on the structure of the chromophore binding pocket. Slight displacements and rotations of His278, His248, Asp190, Tyr205, Arg211, Met163, and Ser262 are predicted. A somewhat larger structural rearrangement occurs in the hydrophobic cavity comprising Phe192, Phe167, and Val175. The BV backbone remains essentially unchanged (RMSD value of 0.26 ± 0.03 Å). Also for this mutant, the simulations revealed a reorientation of prop*C* by about 90° and a minor twisting of ring *D* relative to ring *C* by about 2° compared to the crystal structure of WT Agp2-PCM. The protein matrix around pCNF165 is only slightly affected by the presence of the nitrile group. The largest deviations with respect to the crystallographic arrangement of WT Agp2-PCM are observed for prop*C* (Figure 2D). In the Y165pCNF model, the nitrile group of pCNF165 forms a strong H-bond with His278. This interaction remains stable throughout the 20 ns MD simulations.

Correspondingly, also the RR spectra of the Pfr states of the two variants agree very well with those of the WT protein both with respect to frequencies (± 1 cm^{-1}) and relative intensities (Figures 3, S4 – S6). The only notable exceptions refer to two modes of the *C*-*D* methine bridge in Y165pCNF, i.e., the hydrogen out-of-plane mode (HOOP) at 804 cm^{-1} and the C=C stretching (*C*-*D*) at 1603 cm^{-1} (Figures 3, S5). The respective frequency shifts by −8 and +3 cm^{-1} compared to WT full-length Agp2 (Agp2-fl) correspond to increased dihedral angles of the *C*-*D* methine bridge single and double bond and thus a larger twist of ring *D* in line with the structural model.[20]

Photoinduced structural changes of F192pCNF and Y165pCNF. The far-reaching agreement between the RR spectra of F192pCNF and WT Agp2-fl also holds for the intermediate states. Again, we note only subtle deviations in frequencies and relative intensities for the Lumi-F and Meta-F states (Figures 3, S4, S7). Spectral differences, however, are observed for the Pr state. In WT Agp2-fl, the *ZZZssa* chromophore forms a pH-dependent keto-

enol equilibrium due to the intramolecular proton transfer from the ring *C* nitrogen to the ring *D* C=O group.[6] This is reflected by characteristic RR bands such as those at ca. 1581 and 1252 cm^{-1} as shown in detail in the Supporting Information (Figure S7). Thus, the increased intensity at these positions in the Pr state of F192pCNF indicates a distinctly higher population of the enol tautomer at pH 7.8 than in the WT protein. Beside of the shift of the tautomeric equilibrium, there is no indication for any structural perturbations of the chromophore in the F192pCNF variant.

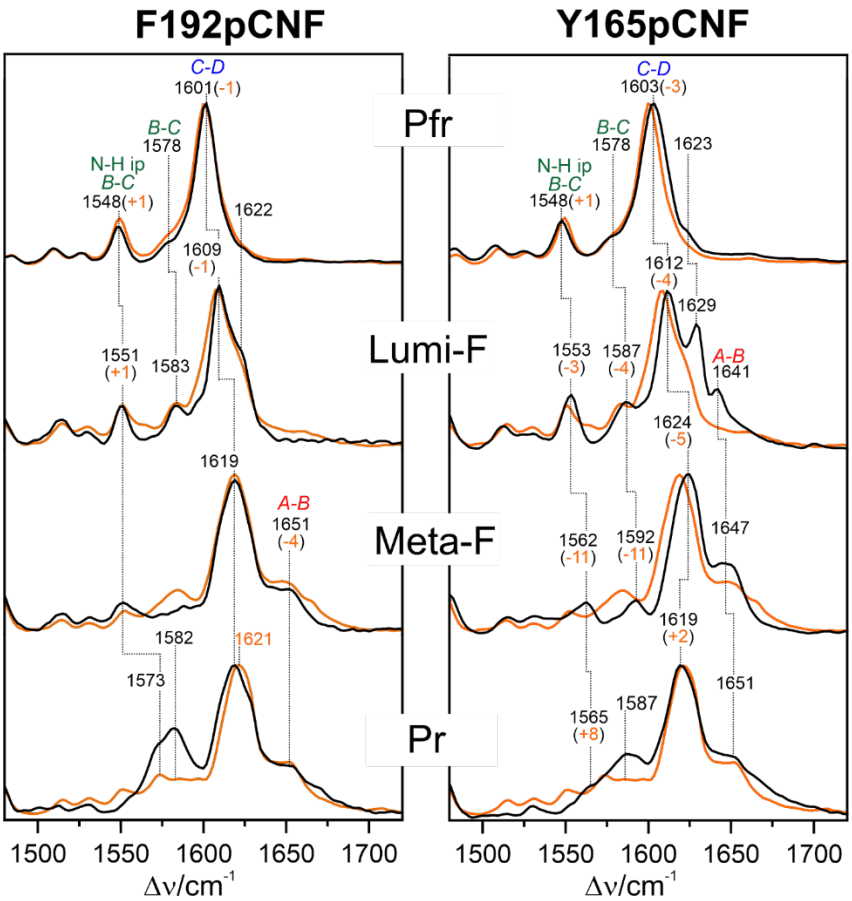

Figure 3. RR spectra of F192pCNF (left) and Y165pCNF (right) of the different states of the Pfr → Pr photoconversion route. The spectra of the variants (black traces) are compared with those of the WT full-length Agp2-fl (orange traces). Black labels refer to the bands of the variant; deviation from the respective values for WT Agp2-fl (in parentheses) are given in orange numbers. The different states were obtained by cryogenic trapping at different temperatures as described in the Experimental section but measured at 80 K. The full range spectra are shown in the Supporting Information (Figures S4 - S8).

The IR difference spectra “Lumi-F/Pfr” and “Meta-F/Pfr” are very similar for F192pCNF and the WT Agp2-PCM (Figure 4).

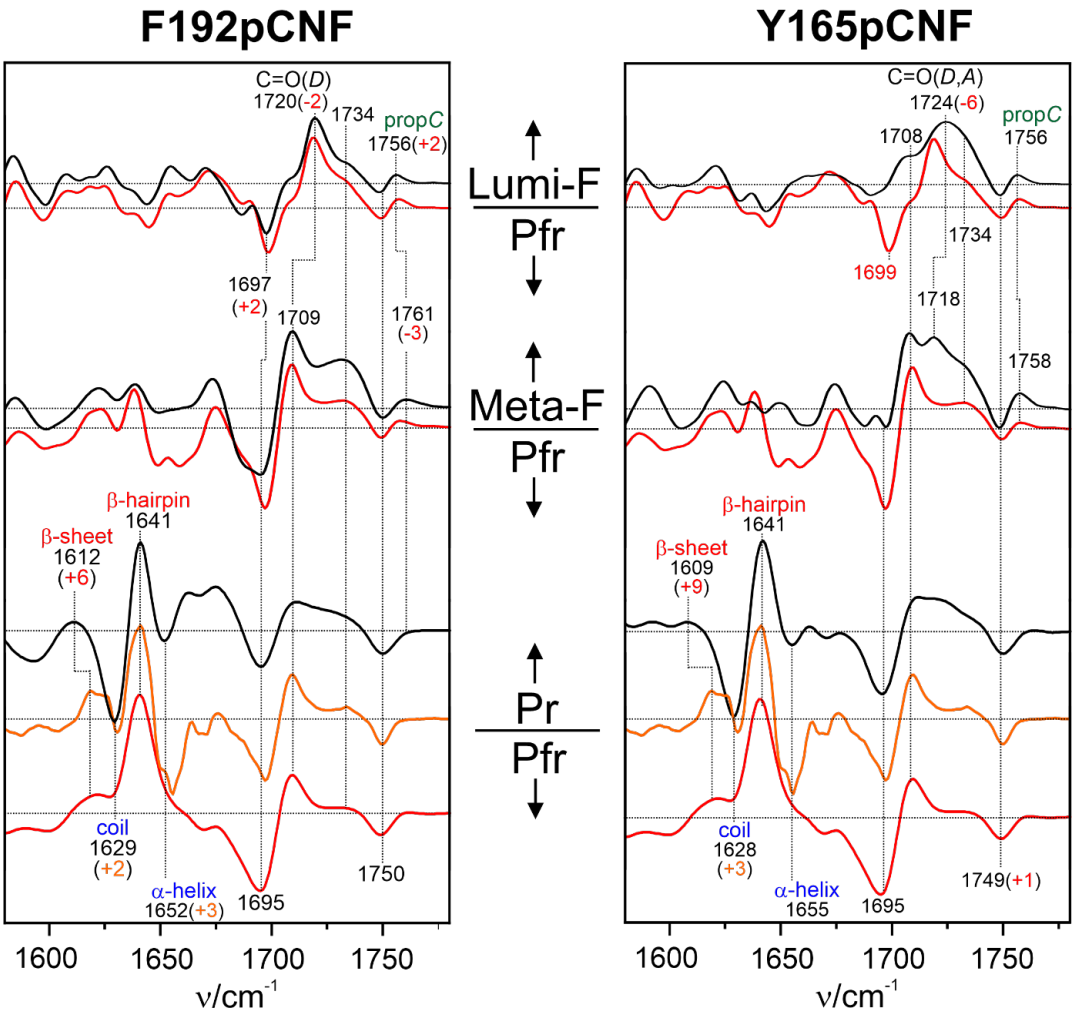

Figure 4. IR difference spectra of F192pCNF (left) and Y165pCNF (right) of the different states of the Pfr → Pr photoconversion route. The spectra of the variants (black traces) are compared with those of the WT Agp2-fl (orange traces) and WT Agp2-PCM (red traces). Black labels refer to the bands of the variant; deviation from the respective values for WT Agp2-fl and WT Agp2-PCM (in parentheses) are given in orange and red numbers, respectively. The photoinduced difference spectra were obtained upon irradiation at different temperatures as described in the Experimental section. As shown in detail previously,[6] the thermal recovery of Pfr, which can proceed via Meta-F and Pr and thus without and with the restructuring of the tongue, respectively,[40] is much faster in Agp2-PCM than in full-length Agp2. Consequently, the Pr/Pfr IR difference spectra of WT Agp2-PCM and Agp2-fl, measured under quasi-photostationary conditions, reflect different relative contributions from Pfr, Meta-F, and Pr. Accordingly, F192pCNF with a life time of Pr (< 60 s) similar to WT Agp2-fl also displays a similar IR difference spectrum.

Specifically, we note that the prop*C* group of the BV remains protonated as indicated by the signal pair at ca. 1750/1760 cm^{-1}, whereas the lack of distinct signals in the amide I band region (1600 – 1680 cm^{-1}) rules out any secondary structure changes of the protein. Conversely, the "Pr/Pfr" difference spectrum of F192pCNF does not show a positive band in the prop*C* band region, indicating deprotonation of this group in Pr as in WT Agp2-PCM and Agp2-fl.[6,8] Furthermore, it displays the expected changes of amide I difference bands that mainly originate from the transition of the coil and α-helical structure of the tongue in Pfr (negative peaks at 1629 and 1652 cm^{-1}, respectively) to the β-sheet and hairpin structure in Pr (positive bands at 1612 and 1641 cm^{-1}, respectively), as discussed in detail previously.[5,6,7,8,14,21] Finally, the reduced intensity at ca. 1709 cm^{-1} (ring *D* C=O stretching) reflects the increased enol content, consistent with the RR spectrum of F192pCNF. Note that the Pr/Pfr IR difference spectrum of F192pCNF is more closely related to the WT Agp2-fl rather than to WT Agp2-PCM since due to the fast thermal Pfr recovery reactions the latter variant includes a much lower Pr contribution under the quasi-photostationary conditions of the experiments.[8,7]

In contrast to F192pCNF, the Y165pCNF variant shows distinct differences in the RR and IR spectra of Lumi-F and Meta-F compared to the WT Agp2. The distinctly different RR spectrum of Lumi-F appears to be the consequence of the increased torsion of the *C-D* methine bridge in the Pfr state of Y165pCNF (Figure 3). As described in detail in the Supporting Information (Figures S5, S6, S8), photoisomerization to Lumi-F leads to a highly distorted *C-D* methine bridge such that the ring *D* mode (including the vinyl stretching coordinate) is significantly upshifted compared to the WT Agp2-fl. These geometry changes are presumably accompanied by local perturbations of the H-bond network around the pCNF165 side chain which in turn affect the interactions of the ring *D* C=O group. The unusually broad IR band in the C=O stretching region at 1708 and 1724 cm^{-1} may also indicate structural heterogeneity of the H-bonding interactions of the ring *D* C=O group (Figure 4).

In the more relaxed chromophore configuration of the Meta-F state, the BV configuration also differs in some details from that of the WT Agp2 as shown by the upshifted *C-D* stretching in the RR spectrum (Figures 3, S8) and the three positive signals in the region of the C=O stretching modes of the IR difference spectrum at 1708, 1718, and 1734 cm^{-1} (Figure 4). Only in the Pr state, the RR and IR spectra are more similar to those of the WT protein (Figures 3, S8). The IR difference spectrum clearly shows the deprotonation of prop*C* and the α-helix to β-sheet conversion of the tongue, similar to the F192pCNF variant. Also the unusually broad and overlapping bands in the C=O stretching region between 1705 and 1735 cm^{-1} have lost intensity, such that the typical negative 1699 cm^{-1} signal of Pfr, presumably obscured in the Lumi-F/Pfr and Meta-F/Pfr IR difference spectra by the adjacent positive 1708 cm^{-1} band, is now detectably in the Pr/Pfr differences spectrum as in the WT protein. Also the RR spectrum of Y165pCNF agrees very well with that of WT Agp2-fl. The enol/keto ratio is only slightly larger than in WT Agp2-fl but smaller than in F192pCNF.

The nitrile stretching mode during the Pfr-to-Pr photoconversion. The nitrile stretching mode responds to both non-covalent electric fields $\left|\vec{E}\right|$ (VSE) and H-bonding.[22,9] The frequency of the mode decreases with increasing electric field strength which can be well described by a linear relationship according to

(1) $\nu = \nu_0 - |\overrightarrow{\Delta\mu}| \cdot \left|\vec{E}\right| \cdot cos\theta$

where ν and ν_0 are the frequencies in the presence and absence of $\left|\vec{E}\right|$, respectively; $|\overrightarrow{\Delta\mu}|$ is the difference dipole moment, pointing along the nitrile bond, and θ is projection angle of the electric field on the difference dipole moment. Conversely, the nitrile stretching frequency increases linearly with increasing strength and/or extent of H-bonding. Thus, high local electric fields and strong H-bonding may counterbalance the effect on the stretching frequency. The two variants studied in work were generated by substituting a residue in a H-bonded environment (Tyr165) and in an environment free of any H-bonding interactions (Phe192).

In the Pfr state of the Y165pCNF variant, the nitrile stretching mode is found at 2240.3 cm^{-1} at 143 K and steadily decreases to 2237.1 cm^{-1} at 298 K (Figure 5).

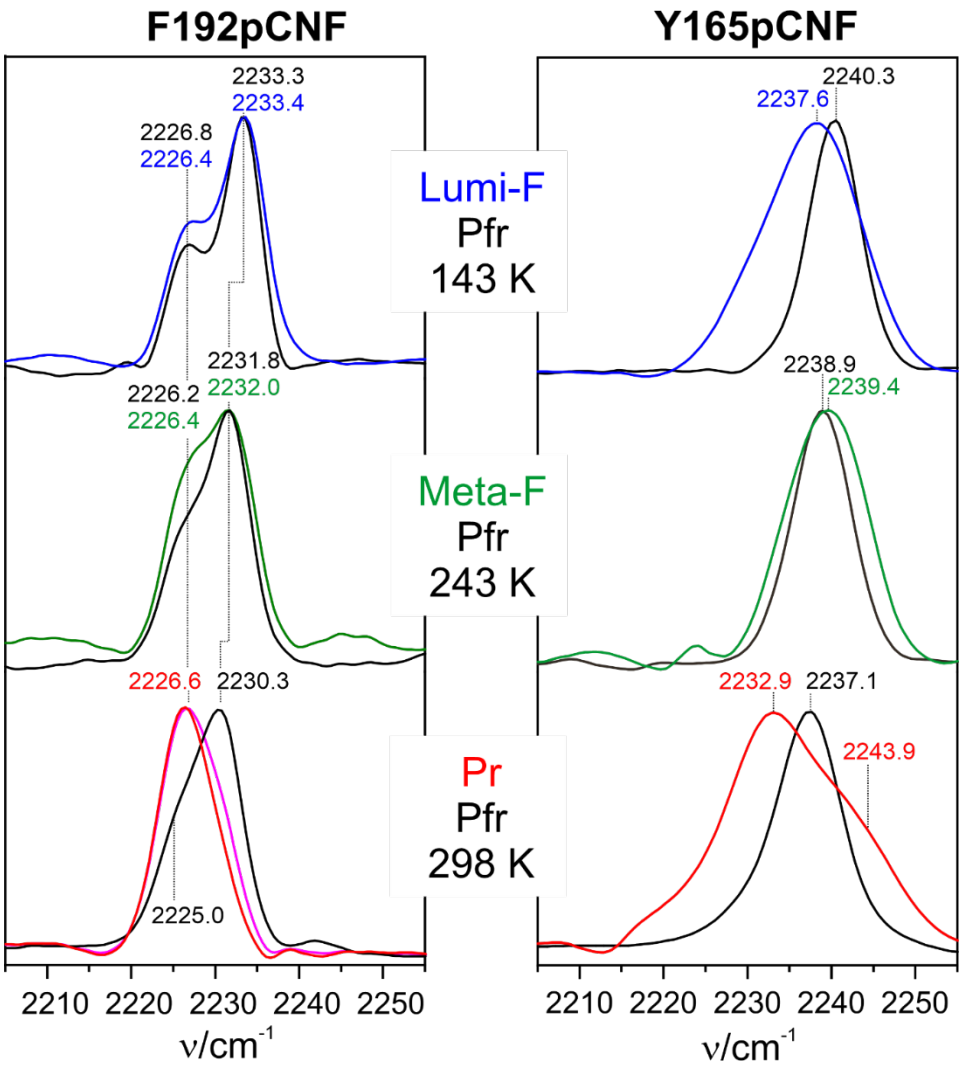

Figure 5. Selection of spectra showing the nitrile stretching bands of F192pCNF (left) and Y165pCNF (right) for the different states of the Pfr → Pr photoconversion, measured at different temperatures (Further spectra are shown in Figures S9 and S10). In each case, the spectrum of the Pr state (black trace) is shown as a reference. The blue, green, and red traces refer to the different intermediates, measured at the indicated temperatures. To obtain the pure spectrum of Pr spectrum of F192pCNF (red trace), a residual contribution (ca. 25%) of Pfr was subtracted from the spectrum measured at ambient temperature (magenta trace). Band positions were determined from fits of Gaussian bandshapes to the spectra.

Transition to the Lumi-F state leads to a significant frequency downshift by –2.7 cm^{-1} which is essentially reversed in Meta-F. Interestingly, the bands of the intermediates are distinctly broader than the corresponding band of Pfr, measured at the same temperature. The most pronounced effects are observed in the Pr state both as a red-shift of –4.2 cm^{-1} and a broadened bandshape, which indicates the existence of a second band component at 2243.9 cm^{-1}. For each spectrum obtained after irradiation, a residual contribution of the non-photolyzed parent state cannot be excluded *a priori*. However, weighted subtraction of the conjugate Pfr spectra leads to artefacts already at relatively small weighting factors such that the non-subtracted spectra of the intermediate states were used for further analysis.

This is also true for the Lumi-F and Meta-F intermediates of F192pCNF (Figure 5) although in these cases both intermediates and the parent Pfr state show a double-banded structure in the nitrile stretching region that was analyzed by band fitting (Figures S9, S10). The frequencies of the two band components of Pfr at ca. 2226 and 2233 cm^{-1} remain largely unchanged in Lumi-F and Meta-F spectra. However, the intensity ratio of the low- to high-frequency band varies compared to the Pfr state. Only for the Pr state of F192pCNF, most likely a small Pfr contribution is included in the spectrum since – in contrast to Y165pCNF – dark reversion is sufficiently fast (data not shown) to establish a notable steady state concentration of Pfr during the IR experiment. Subtraction of ca. 25% of the Pfr spectrum yields in fact a spectrum with only one band which can be well described by a single Gaussian and thus this spectrum is considered as the pure spectrum of Pr where the single nitrile stretching mode is found at a position (2226.6 cm^{-1}) higher than the low-frequency band component of Pfr (2225.0 cm^{-1}). As shown for Pfr, the frequencies of both bands decrease with increasing temperature (Supporting Information, Fig. S11; Table S1) which is in line with previous observations on nitrile VSE reporter groups.[23,24] Assuming that the temperature-dependence of the band

frequencies is similar for all intermediates as in Pfr, the band positions can be normalized to the same temperature (298 K) as listed in Table 1.

Table 1. Band positions of the nitrile stretching modes of the various states of F192pCNF and Y165pCNF normalized to 298 K.[1]

state	F192pCNF		Y165pCNF
	band A / cm^{-1}	band B / cm^{-1}	main band / cm^{-1}
Pfr	2225.0 (–0.010 $cm^{-1}/K)^2$	2230.6 (–0.016 $cm^{-1}/K)^2$	2237.1 (–0.020 $cm^{-1}/K)^2$
Lumi-F	2224.6	2230.7	2234.4
Meta-F	2225.2	2230.8	2237.6
Pr	2226.6	-	2232.9

[1] The temperature-dependence of the nitrile stretching modes of Pfr (Figure S11) was used to extrapolate the frequencies for Lumi-F (measured at 143 K) and Meta-F (measured at 243 K) to 298 K.

[2] Slopes of the linear frequency-temperature relationship of the nitrile stretching modes of Pfr (Figure S11).

Electric field calculations for F192pCNF. Based on the structural model of F192pCNF in the Pfr state (Figure 2) we have calculated the electric field of the protein acting on the nitrile bond of the pCNF side chain as well as the respective nitrile stretching frequency. The calculations were carried out by a hybrid approach in which the chromophore, pCNF192, the side chains of Cys13 and Asp196 as well as the pyrrole water were treated on a quantum mechanical (QM) level whereas for the remainder of the protein and the solvent a molecular mechanical (MM) force field was employed. This QM/MM approach and its successful

validation for benzonitrile in various solvents are described in detail in the Supporting Information (sect. 3.3). The calculations of F192pCNF were then carried out for 50 different QM/MM optimized snapshots of the MD simulation of the Pfr model. The structural differences between the various MD snapshots are very small except for Phe167 that is close to pCNF192 and was found in two main conformations (Figure 6).

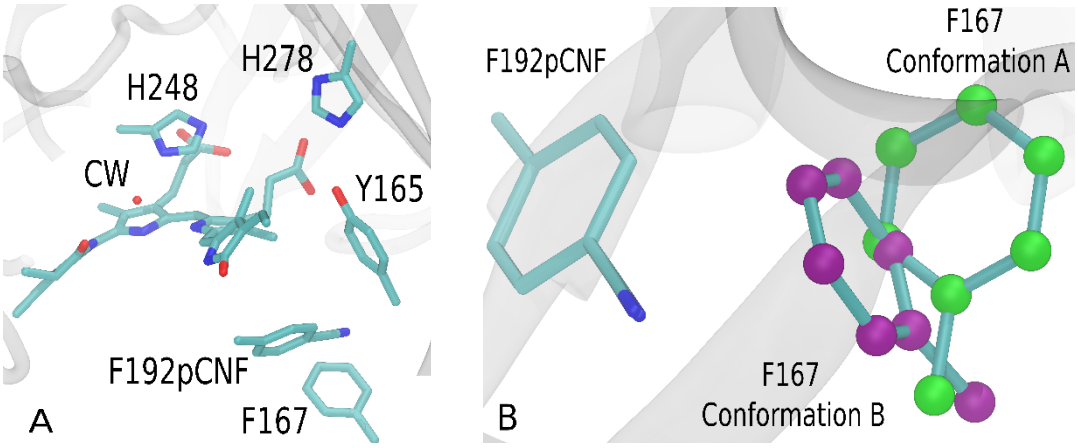

Figure 6. (**A**), overview of the chromophore binding pocket of the F192pCNF variant depicting a representative model in the Pfr state after QM/MM geometry optimization. (**B**), representative structure models of conformations A (green balls) and B (violet balls) of Phe167 in the vicinity of F192pCN after superimpose the heavy atoms of the reporter group F192pCNF.

In the majority of the snapshots (42 out of 50), the phenyl ring of this residue adopts an orientation that is almost perpendicular to the nitrile bond (conformation B) whereas in the remaining eight snapshots parallel orientation is observed (conformation A). This structural difference has consequences for the calculated electric field along the nitrile bond and its stretching frequency which was scaled by a factor 0.953, as derived from the comparison of DFT-calculated and experimental values for benzonitrile in various solvents (Supporting Information, Figure S13A). The QM/MM calculations for the MD snapshots in conformation A yielded frequencies with an average value of 2226.5 cm^{-1} and an average electric field

strength of –23.7 MV/cm^{-1} whereas for the snapshots in conformation B the corresponding values were evaluated to be 2231.1 cm^{-1} and –19.4 MV/cm^{-1} (Figure 7A).

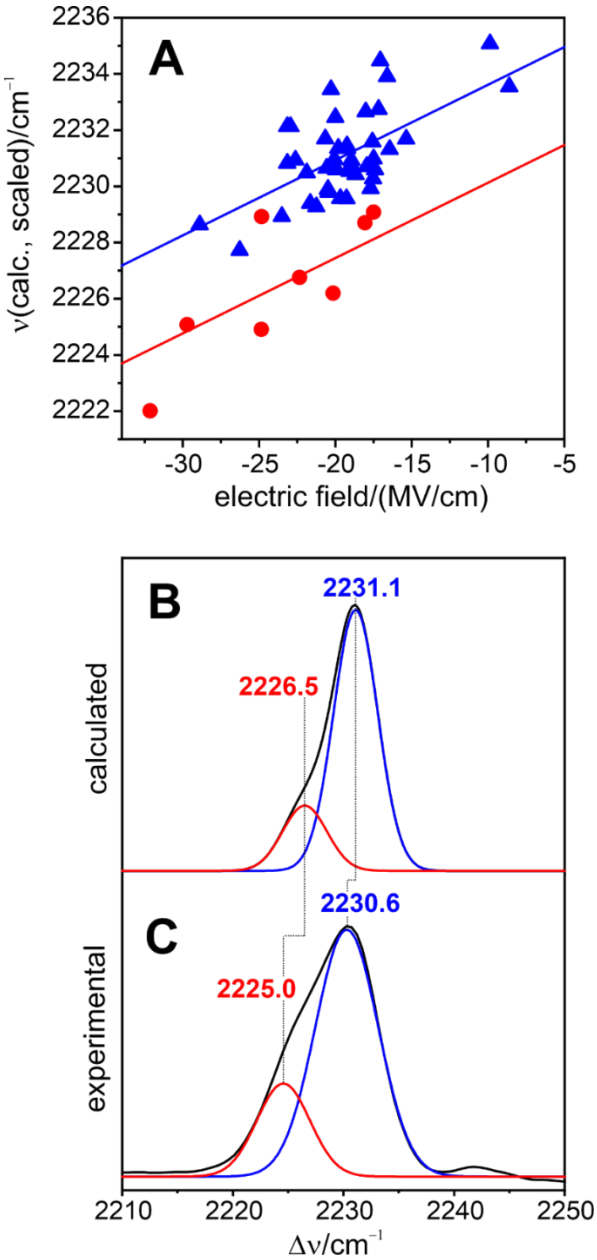

Figure 7. Frequencies of the nitrile stretching mode in the conformation A (red) and B (blue) of the Pfr state of F192pCNF. (**A**), scaled calculated frequencies plotted against the calculated electric strengths. The solid lines represent linear fits using the same slope as determined for the solvent calibration system. (**B**), predicted nitrile stretching profile obtained from the calculated frequencies and the relative incidence of the two populations. The half width was fixed to a value of 8 cm^{-1} similar to that of the experimental bands. (**C**), experimental spectrum including the fit of two Gaussian profiles to the experimental envelope.

All data calculated for both conformations can be described by a linear function with a slope of 0.268 $(MV/cm)^{-1}\cdot cm^{-1}$ (Figure S13). This value was determined from the calibration of the QM/MM approach when simulating benzonitrile in various explicit solvents and is in excellent agreement with the value reported by Deb et al..[22] It also compares very well with the quantity $f \cdot |\overrightarrow{\Delta\mu}| = 0.61\ (MV/cm)^{-1} \cdot cm^{-1}$ determined by Stark spectroscopy, taking into account a correction factor *f* for the local field of ca. 2.[9]

The two conformations revealed by the calculations can readily be related to the two-banded nitrile stretching observed for Pfr. A fit of Gaussian lineshapes to the experimental spectrum at ambient temperature yielded two components at 2230.6 and 2225.0 cm^{-1} (Figure 7C), which is very well reproduced by a spectrum constructed by Gaussian bands using the calculated frequencies of the two conformations and their relative contributions (Figure 7B).

Electric field changes during the photoconversion of F192pCNF. The calculations were extended to the Lumi-F intermediate for which a structural model was generated from the Pfr structure by rotating the *C-D* methine bridge to afford a *ZZZssa* configuration. Also in this case we found both conformers although conformer A is even less populated than in Pfr (Supporting Information, Sect. 4; Figs. S14, S15). The QM/MM calculations of 50 snapshots yielded an average frequency and field strength of 2232.9 cm^{-1} and −18.3 MV/cm. The frequency is similar to that of Pfr, in line with the experimental data. However, the scattering of the data was distinctly larger than in the case of Pfr which we attribute to the uncertainty and fluctuations of the structural model (Table S3).

Any attempts to obtain consistent results for the Meta-F and Pr states failed due to the lack of reliable structural models. For the Meta-F state of F192pCNF, a model was built on the basis of the crystal structure of the Meta-F-like photoproduct of the Agp2-PAiRFP2 (chain A). This structural model lacks a large portion of the tongue region encompassing residues AA439 – AA448 (Supplementary Information, sec. 1.2).[5] According to the crystal structure, the Phe192

side chain flips by about 180° adopting a conformation in which the aromatic ring is oriented towards the tongue region (Figure S15). Therefore, the precise locations of amino acids of parts of the tongue, such as the Asn443, are particularly critical for the electric field calculations on pCNF192. In case of Asn443, slight displacements of the side chain influence the orientation of a water molecule located in H-bond distance to the reporter group. The inaccuracy of the F192pCNF Meta-F structural model is also reflected by the stretching frequencies which are predicted to be at ca. 2234.4 and 2238.5 cm^{-1}, characteristic of non-H-bonded and H-bonded nitrile groups, respectively. These values are much higher than the experimental data which in turn are essentially the same as in Pfr (Figure 5).

Electric field changes in Y165pCNF. Here, the nitrile function is H-bonded in Pfr as shown by the structural model (Figure 2). This is in line with the spectroscopic data since the nitrile stretching displays an unusually high frequency at ambient temperature (2237.1 cm^{-1}) that is even higher than for benzonitrile in water (2233.5 cm^{-1}; Figure S13), and instead reflects the specific H-bonds formed with His278 (Figure 2). As for F192pCNF, we have used the temperature-dependence of the nitrile stretching mode in Pfr to normalize all frequencies to 298 K (Table 1; Supporting Information, Fig. S11; Table S1). Also in Y165pCNF, the most pronounced frequency changes compared to Pfr occur in the last step, the transition to Pr, where the nitrile stretching frequency is lower by 4.2 cm^{-1}.

Discussion

The two variants used in this work contain pCNF at two different positions in the chromophore binding pocket. The impact of the VSE label on the structural integrity is evidently smaller at position 192 than at position 165. When compared to WT Agp2, the RR and IR spectra of F192pCNF rule out notable structural changes of the chromophore and the protein throughout the Pfr $\rightarrow$ Pr phototransformation, whereas the results for Y165pCNF indicate structural

perturbations at the isomerization site of the chromophore that are detectable in Pfr as well as in the Lumi-F and Meta-F intermediates. These structural changes result from the substitution of the hydroxyl by the nitrile group, the function of which primarily alters the hydrogen bonding interactions, substitution of the hydroxyl by the nitrile function, which primarily alters H-bonding interactions as specifically reflected in particular by the spectral changes of the ring *D* C=O stretching (Figure 4). In Pr, Y165pCNF and F192pCNF show a shift of the enol/keto equilibrium up to 3:1 compared to ca. 1:1 in the WT protein.[6] Most importantly, in both variants, the final reaction step of the Pfr → Pr phototransformation is largely unchanged compared to the WT protein and includes the essential mechanistic events required for communicating the photoinduced signal to the output module, i.e. the deprotonation of prop*C* and the refolding of the tongue segment. Thus, in both variants the photoinduced Stark shift changes can provide valuable information about the role of local electric fields for the mechanism of the Pfr → Pr conversion in Agp2.

Conformational equilibrium in F192pCNF. The C≡N stretching doublet observed in Pfr of F192pCNF can be rationalized in terms of two states A (ca. 2225 cm^{-1}) and B (ca. 2233 cm^{-1}) (Figure 5), in which the nitrile bonds experience different electric fields. The underlying structural difference is localized at Phe167 that switches between two orientations with respect to the adjacent nitrile function of pCNF192 (Figure 6). The QM/MM calculations provide an excellent reproduction of the experimental data indicating that the results obtained for Pfr constitute an ideal reference for the analysis of the spectral data of the intermediate states.

The doublet structure of the nitrile stretching is observed for Pfr, Lumi-F, and Meta-F in the entire temperature range studied here (Figure 5, Table S1). Thus it is reasonable to assume that the two conformational states form a thermodynamic equilibrium that does not only depend on the temperature but also on the electrostatic environment of Phe167.[25] For Pfr, the temperature-dependent variations of the conformational equilibrium can be analyzed in terms of enthalpy

and entropy for the transition from B to A, yielding ΔH ≅ –0.3 kJ/mol and ΔS ≅ –7 J/K·mol (Supporting Information, sect. 3.2.; Figure S12). The values are very small, consistent with the rather subtle structural difference.

The electric-field dependence of the B → A transition (accessible via the projection on the C≡N stretching coordinate) can be approximated by comparing the conformational equilibria of Pfr and an intermediate, measured at the same temperature, and evaluating the free Gibbs energy difference $\Delta\Delta G(Pfr - Int)_I$ according to

$$\Delta\Delta G(Pfr - Int)_I = R \cdot T \cdot \left\{ \left(ln \frac{[A]}{[B]} \right)_{Int} - \left(ln \frac{[A]}{[B]} \right)_{Pfr} \right\}_E \quad (2)$$

where the ratio of the two states [A]/[B] is expressed by the intensity ratio of the corresponding nitrile stretching modes (Table S1). Thus, one obtains 0.33 and –0.17 kJ/mol for $\Delta\Delta G(Pfr - LumiF)$ and $\Delta\Delta G(Pfr - MetaF)$, respectively. These relative low energy differences imply that also the changes of the electric field, sensed by the conformation-controlling coordinate of Phe167 but reported by the intensities of the nitrile stretching of pCNF192, are very small for the transitions from Pfr to Lumi-F and Meta-F. Also at the nitrile group of pCNF192 itself, the electric field changes are small as judged from the largely unchanged nitrile stretching frequencies. For the transition to Meta-F, this finding is remarkable. It was shown previously for the Agp2-PAiRFP2 that Phe192 reorients during the life time of Meta-F and its decay to Pr.[5] Since this movement would have a significant effect on both the intensities and frequencies of the nitrile stretching modes, we conclude that the Meta-F state of F192pCNF cryo-trapped in this study corresponds to an early Meta-F intermediate formed prior to reorientation of Phe192(pCNF192).[5]

Conversely, the positional change of pCNF192 can readily account for the spectral changes of the nitrile stretching modes in the Pr state of F192pCNF. First, we note only a single nitrile stretching mode since due the reorientation of pCNF192 the distance with respect to Phe167 increases distinctly such that the conformational states A and B (as shown in Figure 6) do not

exist anymore.[5] Second, the frequency of the nitrile stretching mode is upshifted from 2225.0 cm^{-1} in Pfr to 2226.6 cm^{-1} in Pr, corresponding to a decrease of the local electric field at the nitrile group. At first glance, it appears to be in contradiction with the significant changes of the electrostatics in the vicinity of chromophore during the Meta-F→ Pr transition, mainly due to the proton transfer from prop*C* to His278.[6,8,7] In fact, the expected increase of the electric field in this reaction step may be the origin for the 4 cm^{-1} downshift of the nitrile stretching in Y165pCNF (*vide infra*). Thus, we conclude that the movement of Phe192/pCNF192 during the Meta-F → Pr transition brings the nitrile function into an orientation with lower sensitivity towards the electric field changes in the chromophore pocket.

In this context it is interesting to refer to the recent study by Kurttila et al. who introduced *para*-azidophenylalanine at different positions in the prototypical phytochrome *Dr*BphP from *Deinococcus radiodurans*, among them also the analogous positions studied in this work, i.e. Phe203 (Phe192 in Agp2) and Tyr176 (Tyr165 in Agp2).[26] The frequencies of the azide stretching modes respond to changes of the molecular environment, however, much less sensitive to variations of the electric field in a quantifiable fashion.[27,28,29] Instead, the azide modes are considered as rather qualitative sensors for polarity changes. Nevertheless, for *Dr*BphP a significant downshift of the azide stretching mode from Pr → Pfr was reported and interpreted in terms of an increased polarity in Pfr.[26] In fact, the present results on Agp2 indicate an increased electric field at the nitrile group of pCNF192 in Pfr compared to Pr but in both states the stretching frequency points to a largely hydrophobic molecular environment. However, it may well be that the Pfr state of the prototypical *Dr*BphP exhibits a less hydrophobic pocket around Phe203 or that the azide label perturbs the preservation of this pocket during the photoconversion.

Hydrogen bonding and electric field changes in Y165pCNF. For this variant, the involvement of the nitrile group in H-bonding interactions impairs a quantitative QM/MM-

assisted analysis of the electric field effects on the nitrile group. In general, quantification of local electric field strengths is yet hardly possible, neither by theoretical nor empirical approaches, since H-bonding and non-covalent electric field effects have partly opposite consequences on the nitrile stretching frequency.[22,9,13] However, making use of previous analyses,[24,30,31] one may characterize the type of H-bonding interactions, specifically distinguishing between *(i)* fluctuating interactions with water molecules and *(ii)* geometrically restricted H-bonding interactions with "fixed" H-bond donors. Nitrile groups in restricted H-bonding interactions display a temperature dependence of the frequency with a small slope (<|–0.03 |cm^{-1}/K) compared to solvent-exposed nitrile functions (Supporting Information, Figure S11).[24] For the Pfr state of Y165pCNF, the slope was determined to be –0.02 cm^{-1}/K which is indeed consistent with a restricted H-bond to His278 as revealed by the structural model (Figure 2D). For the corresponding bands of the Pfr state of F192pCNF even less steep slopes (–0.01 and –0.016 cm^{-1}/K) were found, reflecting the lack of any H-bonding interactions.

Upon transition from the Pfr to the Lumi-F state of Y165pCNF, we observe a downshift of the nitrile stretching from 2237.1 to 2234.4 cm^{-1} accompanied by a substantial broadening of the symmetric bandshape. These changes presumably reflect a reorientation of the H-bond with His278 caused by the rotation of ring *D* upon $E \rightarrow Z$ isomerization of the *C-D* methine bridge. As a consequence, this interaction is less restricted and may involve an increased distribution of slightly different H-bond geometries accounting for the increased bandwidth.[24] The structural relaxation of the chromophore and its immediate environment in Meta-F seems to be also reflected by the nitrile stretching which shows nearly the same frequency and a similar bandwidth as Pfr. In Pr, the main peak is observed at 2232.9 cm^{-1} and thus downshifted by 4.2 cm^{-1} compared to Pfr. The bandshape now adopts a clearly asymmetric and broad envelope and an acceptable fit required at least three components, pointing to heterogeneous H-bonding

structures. The heterogeneity may in part be related to the keto-enol equilibrium since each tautomer may undergo specific H-bonding interactions with His278.[6] Furthermore, it is possible that water molecules have entered the chromophore binding pocket in Pr such that also fluctuating H-bonding contacts contribute to the unusually broad bandshape. Again, the present results are not readily compatible with the conclusions derived from the *Dr*BphP variant carrying *para*-azidophenylalanine at the analogous position Tyr176.[26] In that study, the authors interpreted the data in terms of significantly reduced H-bonding interactions in Pr compared to Pfr.

Electric field effects during the phototransformation of Agp2. In both F192pCNF and Y165pCNF the most pronounced changes of the nitrile stretching modes occur in the last step of the Pfr → Pr photoconversion, i.e. the transition from Meta-F to Pr. These changes take place concomitantly to the proton transfer from prop*C* to His278, which represents a charge separation and thus should be associated with a large change in the electric field, at least along the axis connecting proton donor and acceptor. It is therefore likely to relate the spectral changes in the nitrile stretching region of both pCNF-modified variants in the Pr state to the altered electrostatics in the chromophore pocket. However, in both variants the analysis of the VSE groups faces severe difficulties. Whereas in F192pCNF, the position of the nitrile group seems to be unfavorable to monitor electric field changes, in Y165pCNF the substantial frequency downshift of the main nitrile stretching band from Pfr to Pr may not only reflect an increased electric field strength along the nitrile bond but also alterations of the H-bond geometry.

In previous studies we have demonstrated the importance of the proton-coupled changes of the electrostatics in the chromophore pocket for the signal transfer.[7,8] Specifically, tongue restructuring that is essential for the communication between the PCM and the output module requires the proton translocation from prop*C*. We therefore ask if there is a causal relationship between the secondary structure transition and the electric field change. In fact, an electric field induced transition from an α-helical to a β-sheet structure can readily be rationalized in view

of the quite different dipole moments. Taking into account that dipole moments up to 100 Debye may be associated with α-helical segments of ca. 20 to 25 amino acid residues but close to zero for a β-sheet segment,[32,33,34,35] a change in the electric field by ca. 7.5 MV/cm may correspond to an energy of more than 100 kJ/mol by which one of the structures may be stabilized or destabilized over the other structure, depending on the relative orientation of the field vector with respect to the dipole moment. In fact, electric-field induced structural changes of peptides and proteins have been already proposed and demonstrated in previous experimental and theoretical studies.[36,37,38,39] Specifically, the magnitude of the electric field between 1 and 6 MV/cm predicted to unfold or refold peptide segments including α-helices peptide is quite comparable to the electric field changes that occur in the chromophore binding pocket of Agp2.[33,32,38] For instance, electric field changes of 7.5 MV/cm would correspond to frequency shifts of ca. 4 cm^{-1}. Shifts of this magnitude were in fact found for the main nitrile stretching modes during the last step of the Pfr → Pr photoconversion of both F192pCNF and Y165pCNF, although in the latter case the interference with H-bonding effects impairs a direct correlation with the electric field strength.

Conclusions

The present multidisciplinary approach demonstrates that QM/MM calculations can provide an excellent description for experimentally determined VSE. As a *conditio sine qua non*, however, a reliable structural model derived from crystallographic data is required as it is the case for the Pfr state of Agp2-PCM. Thus, the theoretical simulations reproduced the doubled-banded structure of the nitrile stretching mode with a striking accuracy. In this sense, the results obtained for Pfr could serve as a sound reference for interpreting the spectra obtained from other intermediates, for which no appropriate structural data were available.

In contrast to F192pCNF, the nitrile group of Y165pCNF is involved in H-bonding interactions in all states of the phototransformation. This imposes severe restrictions on the interpretation of the spectroscopic data since the direct translation of frequency shifts into electric field changes is not possible. However, there is a second obstacle that aggravates the determination of electric field effects on specific processes in the protein such as the refolding of a peptide segment. The VSE is a strictly local effect and allows determining the electric field along the nitrile bond whereas conclusions about the electrostatics in the immediate molecular environment cannot readily be derived from the data. Thus, the fact that in both variants the largest VSEs are observed with the decay from Meta-F to Pr is consistent with the hypothesis that the proton-coupled increase of the electric field in the chromophore pocket induced restructuring of the PHY tongue. However, it does not provide an independent proof for this view. Here future studies must aim at proper positioning and orientation of the VSE reporter groups.

Supporting Information

Details about experimental and computational methods, further RR spectra and IR spectra, analyses of the vibrational Stark effect, structural models of the variants. This material is available free of charge via the Internet at http://pubs.acs.org.

Acknowledgements

This work was supported by the Deutsche Forschungsgemeinschaft (DFG) through CRC 1078 (C2 to M.A.M.; B6 to P.S. and P.H.; B9 to J.K.) and through the cluster of excellence "UniSysCat" under Germany´s Excellence Strategy-EXC2008/1-390540038 to I.Z., P.S., M.A.M., N.B. and P.H.. Further support was obtained from the Einstein Center of Catalysis EC2 (to I.Z., P.S., M.A.M and P.H.).

UniProt accession code

Agp2: Q8UDG1

References

(1) Briggs, W. R., and Rice, H. V. (1972) Phytochrome: Chemical and Physical Properties and Mechanism of Action. *Annu. Rev. Plant Physiol. 23*, 293–334.

(2) Rockwell, N. C., Su, Y.-S., and Lagarias, J. C. (2006) Phytochrome Structure and Signaling Mechanisms. *Annu. Rev. Plant Biol. 57*, 837–858.

(3) Yang, X., Ren, Z., Kuk, J., and Moffat, K. (2011) Temperature-scan cryocrystallography reveals reaction intermediates in bacteriophytochrome. *Nature 479*, 428–431.

(4) Takala, H., Björling, A., Berntsson, O., Lehtivuori, H., Niebling, S., Hoernke, M., Kosheleva, I., Henning, R., Menzel, A., Ihalainen, J. A., and Westenhoff, S. (2014) Signal amplification and transduction in phytochrome photosensors. *Nature 509*, 245–248.

(5) Schmidt, A., Sauthof, L., Szczepek, M., Lopez, M. F., Velazquez Escobar, F., Qureshi, B. M., Michael, N., Buhrke, D., Stevens, T., Kwiatkowski, D., von Stetten, D., Mroginski, M. A., Krauß, N., Lamparter, T., Hildebrandt, P., and Scheerer, P. (2018) Structural snapshot of a bacterial phytochrome in its functional intermediate state. *Nat. Commun. 9*, 1–13.

(6) Velazquez Escobar, F., Piwowarski, P., Salewski, J., Michael, N., Fernandez Lopez, M., Rupp, A., Qureshi, M. B., Scheerer, P., Bartl, F., Frankenberg-Dinkel, N., Siebert, F., Mroginski, M. A., and Hildebrandt, P. (2015) A protonation-coupled feedback mechanism controls the signalling process in bathy phytochromes. *Nat. Chem. 7*, 423–430.

(7) Fernandez Lopez, M., Nguyen, A. D., Velazquez Escobar, F., González, R., Michael, N., Nogacz, Ż., Piwowarski, P., Bartl, F., Siebert, F., Heise, I., Scheerer, P., Gärtner, W., Mroginski, M. A., and Hildebrandt, P. (2019) Role of the Propionic Side Chains for the

Photoconversion of Bacterial Phytochromes. *Biochemistry 58*, 3504–3519.

(8) Kraskov, A., Nguyen, A. D., Goerling, J., Buhrke, D., Velazquez Escobar, F., Fernandez Lopez, M., Michael, N., Sauthof, L., Schmidt, A., Piwowarski, P., Yang, Y., Stensitzki, T., Adam, S., Bartl, F., Schapiro, I., Heyne, K., Siebert, F., Scheerer, P., Mroginski, M. A., and Hildebrandt, P. (2020) Intramolecular Proton Transfer Controls Protein Structural Changes in Phytochrome. *Biochemistry 59*, 1023–1037.

(9) Fried, S. D., and Boxer, S. G. (2015) Measuring electric fields and noncovalent interactions using the vibrational stark effect. *Acc. Chem. Res. 48*, 998–1006.

(10) Fafarman, A. T., Webb, L. J., Chuang, J. I., and Boxer, S. G. (2006) Site-specific conversion of cysteine thiols into thiocyanate creates an IR probe for electric fields in proteins. *J. Am. Chem. Soc. 128*, 13356–13357.

(11) Young, D. D., Young, T. S., Jahnz, M., Ahmad, I., Spraggon, G., and Schultz, P. G. (2011) An evolved aminoacyl-tRNA synthetase with atypical polysubstrate specificity. *Biochemistry 50*, 1894–1900.

(12) Völler, J., Biava, H., Koksch, B., Hildebrandt, P., and Budisa, N. (2015) Orthogonal translation meets electron transfer: In vivo labeling of cytochrome c for probing local electric fields. *ChemBioChem 16*, 742–745.

(13) Biava, H., Schreiber, T., Katz, S., Völler, J. S., Stolarski, M., Schulz, C., Michael, N., Budisa, N., Kozuch, J., Utesch, T., and Hildebrandt, P. (2018) Long-Range Modulations of Electric Fields in Proteins. *J. Phys. Chem. B 122*, 8330–8342.

(14) Merga, G., Fernandez Lopez, M., Fischer, P., Piwowarski, P., Nogacz, Z., Kraskov, A., Buhrke, D., Velazquez Escobar, F., Michael, N., Síebert, F., Scheerer, P., Bartl, F., and Hildebrandt, P. (2021) Light- and Temperature-dependent Dynamics of Chromophore and Protein Structural Changes in Bathy Phytochrome Agp2. *Phys. Chem. Chem. Phys. 23*, 18197-18205.

(15) Waterhouse, A., Bertoni, M., Bienert, S., Studer, G., Tauriello, G., Gumienny, R., Heer,

F. T., De Beer, T. A. P., Rempfer, C., Bordoli, L., Lepore, R., and Schwede, T. (2018) SWISS-MODEL: Homology modelling of protein structures and complexes. *Nucleic Acids Res. 46*, W296–W303.

(16) Kieseritzky, G., and Knapp, E. W. (2008) Optimizing pKA computation in proteins with pH adapted conformations. *Proteins 71*, 1335–1348.

(17) Phillips, J. C., Braun, R., Wang, W., Gumbart, J., Tajkhorshid, E., Villa, E., Chipot, C., Skeel, R. D., Kalé, L., and Schulten, K. (2005) Scalable molecular dynamics with NAMD. *J. Comput. Chem. 26*, 1781–1802.

(18) MacKerell, A. D., Banavali, N., and Foloppe, N. (2001) Development and current status of the CHARMM force field for nucleic acids. *Biopolymers 56*, 257–265.

(19) Mroginski, M. A., Mark, F., Thiel, W., and Hildebrandt, P. (2007) Quantum mechanics/molecular mechanics calculation of the Raman spectra of the phycocyanobilin chromophore in α-C-phycocyanin. *Biophys. J. 93*, 1885–1894.

(20) Salewski, J., Escobar, F. V., Kaminski, S., Von Stetten, D., Keidel, A., Rippers, Y., Michael, N., Scheerer, P., Piwowarski, P., Bartl, F., Frankenberg-Dinkel, N., Ringsdorf, S., Gaïtner, W., Lamparter, T., Mroginski, M. A., and Hildebrandt, P. (2013) Structure of the biliverdin cofactor in the Pfr state of bathy and prototypical phytochromes. *J. Biol. Chem. 288*, 16800–16814.

(21) Stojković, E. A., Toh, K. C., Alexandre, M. T. A., Baclayon, M., Moffat, K., and Kennis, J. T. M. (2014) FTIR spectroscopy revealing light-dependent refolding of the conserved tongue region of bacteriophytochrome. *J. Phys. Chem. Lett. 5*, 2512–2515.

(22) Deb, P., Haldar, T., Kashid, S. M., Banerjee, S., Chakrabarty, S., and Bagchi, S. (2016) Correlating nitrile IR frequencies to local electrostatics quantifies noncovalent interactions of peptides and proteins. *J. Phys. Chem. B 120*, 4034–4046.

(23) Adhikary, R., Zimmermann, J., Dawson, P. E., and Romesberg, F. E. (2015) Temperature Dependence of CN and SCN IR Absorptions Facilitates Their Interpretation and

Use as Probes of Proteins. *Anal. Chem. 87*, 11561–11567.

(24) First, J. T., Slocum, J. D., and Webb, L. J. (2018) Quantifying the Effects of Hydrogen Bonding on Nitrile Frequencies in GFP: Beyond Solvent Exposure. *J. Phys. Chem. B 122*, 6733–6743.

(25) Neumann, E. (1986) Chemical electric field effects in biological macromolecules. *Prog. Biophys. Mol. Biol. 47*, 197–231.

(26) Kurttila, M., Stucki-Buchli, B., Rumfeldt, J., Schroeder, L., Häkkänen, H., Liukkonen, A., Takala, H., Kottke, T., and Ihalainen, J. A. (2021) Site-by-site tracking of signal transduction in an azidophenylalanine-labeled bacteriophytochrome with step-scan FTIR spectroscopy. *Phys. Chem. Chem. Phys. 23*, 5615–5628.

(27) Suydam, I. T., and Boxer, S. G. (2003) Vibrational Stark Effects Calibrate the Sensitivity of Vibrational Probes for Electric Fields in Proteins. *Biochemistry 42*, 12050–12055.

(28) Silverman, L. N., Pitzer, M. E., Ankomah, P. O., Boxer, S. G., and Fenlon, E. E. (2007) Vibrational stark effect probes for nucleic acids. *J. Phys. Chem. B 111*, 11611–11613.

(29) Krause, B. S., Kaufmann, J. C. D., Kuhne, J., Vierock, J., Huber, T., Sakmar, T. P., Gerwert, K., Bartl, F. J., and Hegemann, P. (2019) Tracking Pore Hydration in Channelrhodopsin by Site-Directed Infrared-Active Azido Probes. *Biochemistry 58*, 1275–1286.

(30) Slocum, J. D., and Webb, L. J. (2016) Nitrile Probes of Electric Field Agree with Independently Measured Fields in Green Fluorescent Protein even in the Presence of Hydrogen Bonding. *J. Am. Chem. Soc. 138*, 6561–6570.

(31) Farfarman, A. T., Sigala, P. A., Herschlag, D., and Boxer, S. G. (2010) Decomposition of Vibrational Shifts of Nitriles into Electrostatic and Hydrogen Bonding Effects. *J. Am. Chem. Soc. 132*, 12811–12813.

(32) Solomentsev, G. Y., English, N. J., and Mooney, D. A. (2012) Effects of external electromagnetic fields on the conformational sampling of a short alanine peptide. *J. Comput.*

Chem. 33, 917–923.

(33) Wang, X., Li, Y., He, X., Chen, S., and Zhang, J. Z. H. (2014) Effect of strong electric field on the conformational integrity of insulin. *J. Phys. Chem. A 118*, 8942–8952.

(34) Pandey, G., Saikia, J., Sasidharan, S., Joshi, D. C., Thota, S., Nemade, H. B., Chaudhary, N., and Ramakrishnan, V. (2017) Modulation of peptide based nano-assemblies with electric and magnetic fields. *Sci. Rep. 7*, 1–9.

(35) Wang, X., Li, Y., He, X., Chen, S., and Z. H. Zhang, J. (2014) Effect of Strong Electric Field on the Conformational Integrity of Insulin. *J. Phys. Chem. A 118*, 8942–8952.

(36) Schwarz, G., and Seelig, J. (1968) Kinetic Properties and the Electric Field Effect of the Helix-Coil Transition of Poly(y-benzyl L-Glutamate) Determined from Dielectric Relaxation Experiments. *Biopolymers 6*, 1263–1277.

(37) Ojeda-May, P., and Garcia, M. E. (2010) Electric field-driven disruption of a native β-sheet protein conformation and generation of a helix-structure. *Biophys. J. 99*, 595–599.

(38) Jiang, Z., You, L., Dou, W., Sun, T., and Xu, P. (2019) Effects of an electric field on the conformational transition of the protein: A molecular dynamics simulation study. *Polymers (Basel). 11*.

(39) Ilieva, S., Cheshmedzhieva, D., and Dudev, T. (2019) Electric field influence on the helical structure of peptides: Insights from DFT/PCM computations. *Phys. Chem. Chem. Phys. 21*, 16198–16206.

(40) Buhrke, D., Kuhlmann, U., Michael, N., and Hildebrandt, P. (2018) The Photoconversion of Phytochrome Includes an Unproductive Shunt Reaction Pathway. *ChemPhysChem 19*, 566–570.